SCIENCE CHINA
Information Sciences

• RESEARCH PAPER •

June 2024, Vol. 67, Iss. 6, 162201:1–162201:14
https://doi.org/10.1007/s11432-023-3923-8

Adaptive observer-based integral event-triggered antivibration control of a full aircraft active landing gear system with irregular runway excitations

Wenxiao HU[1,2], Chenglong DU[1*], Fanbiao LI[1], Xinmin CHEN[2], Chunhua YANG[1] & Weihua GUI[1]

[1]*School of Automation, Central South University, Changsha* 410083*, China;*
[2]*Research Center in System Engineering for Special Aircrafts, Ningbo Institute of Materials Technology and Engineering, Chinese Academy of Sciences, Ningbo* 315201*, China*

Received 6 May 2023/Revised 1 September 2023/Accepted 28 September 2023/Published online 13 May 2024

Abstract This study addresses the antivibration issue of a full aircraft active landing gear system (LGS) under landing impact and runway excitations via a novel adaptive observer-based integral event-triggered control method. First, a full aircraft active LGS comprising a front gear and two synchronized main left and right gears with active suspensions is established, where the information exchange among them is not implemented directly. Second, two adaptive observers are designed separately for the front and main LGSs to identify the varying damping parameters and estimate the system states simultaneously. Third, estimated states are transmitted to a shared network through a novel integral event-triggered mechanism (I-ETM); thus, the front and main LGSs are interconnected, and a networked control scheme for the aircraft LGS is constructed. Additionally, the integrated active control law is designed with the aid of the transmitted states of the front and main LGSs, enhancing the robustness against the pitch vibration of the aircraft. Furthermore, the $\mathcal{L}_2$-stability of the hybrid system is guaranteed to depress the vertical vibration effect of the landing impact and irregular runway excitations, thus improving passenger safety and comfort. Moreover, a codesign method is provided to obtain feasible solutions to the gain matrices of the observers and controllers simultaneously. Simulation and comparison results are presented to illustrate the effectiveness and superiority of the proposed control scheme in antivibration and saving communication resources.

Keywords aircraft active landing gear, antivibration control, integral event-triggered mechanism, adaptive observer, $\mathcal{L}_2$-stability

1 Introduction

Antivibration control during aircraft landing and taxiing is a critical concern to be seriously addressed because vibrations caused by landing impact and runway irregularity affect the safety and comfort of crewmembers and passengers and the lifespan of the aircraft [1]. The landing gear system (LGS), as a bridge connecting the aircraft fuselage and wheels, aims to absorb and dissipate the landing kinetic energy quickly to retard the transmission of vibrations induced by landing impact and runway excitations to the aircraft fuselage. In addition to the property of dissipating vertical energy, the aircraft LGS should ensure stability and maneuverability after landing [2]. In most cases, passive damping devices installed in aircraft LGSs can absorb some landing energy, but their suspension performance is greatly affected by runway characteristics and impact loads, which cannot provide a reliable guarantee for the safety and comfort of crewmembers and passengers. The reason is that the stiffness and damping of the passive damping devices cannot adapt to different types of runway excitations and impacts. Therefore, many semiactive and active suspension systems integrated with various control methods have attracted considerable attention in aircraft and vehicles, such as H_∞ control [3,4], adaptive backstepping control [5], event-triggered control [6–8], sliding mode control [9], predictive control [10], fuzzy logic control [11], and neural network-based control [12].

* Corresponding author (email: chenglong_du@csu.edu.cn)

To study the antivibration problem of aircraft during landing or taxiing processes, several aircraft-on-ground models have been established [5, 9, 13–16]. For example, a single landing gear system of an aircraft is established in [5], in which the aircraft is taxiing straight and only the vertical vibration induced by runway irregularity is considered. Furthermore, the landing gear system is built taking the landing impact into account, but only the vertical dynamics is considered [14]. However, three landing gears are distributed in the front, the left, and the right of the aircraft, and different vertical displacements and/or acceleration of the gears would cause pitch and/or yaw vibrations to the aircraft. Therefore, a full aircraft-on-ground model with vertical, pitch, and yaw dynamics is developed in this study; thus, vibrations from the vertical, pitch, and yaw directions can be further investigated [9, 16, 17].

Moreover, the information exchange between the front and main LGSs cannot be implemented directly; that is, the control signals generated by the suspensions of the front and main LGSs are independent [1, 17]. Furthermore, only the displacement of the junction of the aircraft fuselage and the front/main landing gears and the displacement of the front/main landing gears are measurable and accessible for each LGS. However, the damping parameters of the front and main landing gears and wheels vary during aircraft landing and taxiing processes, degrading model accuracy and affecting control performances [9,16]. Therefore, two adaptive observers are designed separately for the front and main LGSs in this study to estimate the system states and identify the damping parameters of gears and wheels. Subsequently, estimated states of the front and main LGSs are transmitted to a shared network; thus, the front and main LGSs are interconnected, and the information exchange among them is realized. Furthermore, the integrated active controller is designed fully considering the interconnection of the two subsystems, rather than designing controllers separately for each subsystem, thus improving the robustness against the pitch vibration of the aircraft. Finally, a networked control system (NCS) for the aircraft LGS is constructed.

Generally, the network bandwidth of the NCS is limited, and network congestion may occur [18]. Considerable efforts have been made to save more network communication resources, such as [3, 8, 19–21] and the references therein. The sampled-data system has been widely used because of its potential to reduce the signal transmission frequency of NCS [21–23]. However, traditional sampled-data systems, such as periodic sampled-data systems, have limited ability to reduce network communication and may lead to system instability when unexpected disturbances or faults occur [22, 23]. Therefore, an event-triggered networked control scheme is proposed in which signal transmission is only performed when the triggering condition is violated [22–27]. Nevertheless, the abovementioned event-triggered mechanisms (ETMs), namely, static event-triggered mechanisms (S-ETMs), require the Lyapunov function to decrease monotonically over time. However, this restriction could be lifted from the stability perspective; that is, the stability of the closed-loop system can be guaranteed by ensuring that the storage function between two successive triggering instants is nonincreasing [28, 29]. In contrast to S-ETMs, the dynamic ETM proposed in [30] introduces an internal variable to construct the triggering condition, which can further enlarge the interevent time and save more communication resources. When the parameter θ in [30] is zero, it becomes an integral event-triggered mechanism (I-ETM), and the duration between two triggering instants reaches the maximum. Other extensions based on dynamic/integral ETMs can be referred to [11, 20, 21, 31–34]. We propose a novel I-ETM in this study to regulate signal transmission from the observer to the shared network, aiming to save more network communication resources under the premise of ensuring system stability and antivibration performance. Moreover, the $\mathcal{L}_2$-stability of the closed-loop system will be implemented to guarantee system robustness from runway excitations to the vertical displacement and acceleration of the LGS, thus depressing the vertical vibration effect. A codesign method with an adaptive law is further provided to obtain feasible solutions to the gain matrices of the controller and observers.

First, a full aircraft LGS composed of a front landing gear subsystem and a subsystem of two synchronized main landing gears is established, where the vertical and pitch dynamics are considered, and information exchange between subsystems is realized over a shared network.

Second, two adaptive observers are designed separately to estimate subsystem states and simultaneously identify varying damping parameters of the system. Additionally, a novel I-ETM at the observer-to-network channel is synthesized to save more communication resources of the NCS under the premise of ensuring system stability and antivibration performance.

Moreover, the integrated active controller, instead of designing controllers for each subsystem separately, fully considers the interconnection of subsystems, thus improving the robustness against the pitching vibration of the aircraft.

Finally, the $\mathcal{L}_2$-stability of the hybrid system is guaranteed to improve the system robustness from

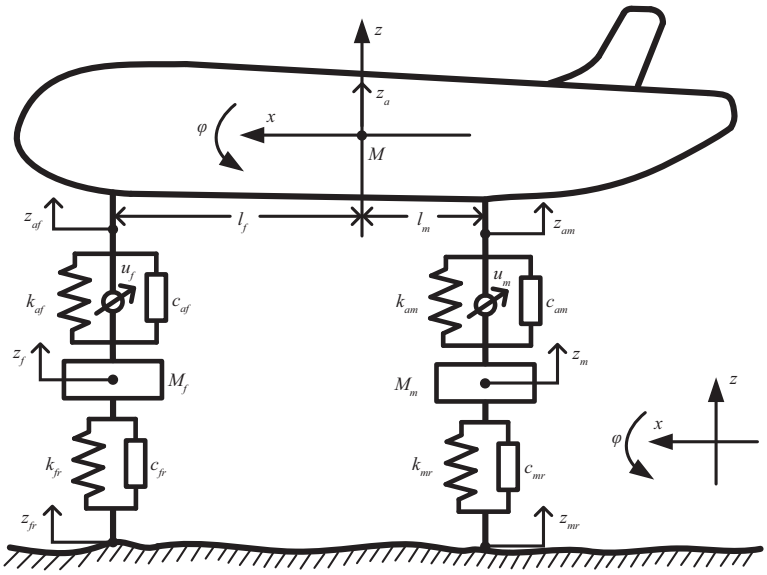

Figure 1 Force diagram of full aircraft LGS with active suspensions.

runway excitations to the vertical displacement and acceleration of the LGS. Furthermore, a codesign method is provided to obtain feasible solutions to the gain matrices of observers and the controller simultaneously.

Notations. $\mathbb{R}$, $\mathbb{R}_{\geqslant 0}$, and $\mathbb{Z}_{\geqslant 0}$ denote the real number, nonnegative real number, and nonnegative integer sets, respectively. $\mathbb{R}^{n\times m}$ stands for the set of all real matrices of dimensions $n\times m$. The transposed matrix is expressed by the matrix superscript T. The zero matrix with appropriate dimensions is represented by O, and the identity matrix with $n\times n$ dimensions is described by I_n. $P>0$ or $P\geqslant 0$ indicates that P is a positive/semi-positive definite symmetric matrix. $\mathrm{diag}\{\cdots\}$ symbolizes the block diagonal matrix. The 2-norm of a vector is defined as $\|\cdot\|$. $\langle\Upsilon, F\rangle$ stands for the time derivative of Υ along with the flow F. The notation inf represents the minimum of a function. A continuous function ϱ is of class $\mathcal{K}_\infty$ if it strictly increases with $\varrho(0)=0$ and $\varrho(s)=\infty$ as $s\to\infty$. For any variable or variable vector, if not mentioned, the argument t is omitted.

2 Modeling of the full aircraft landing gear system

The full aircraft LGS comprises a front landing gear subsystem and a subsystem of two synchronized main landing gears, and a force diagram of the full aircraft LGS with active suspensions is shown in Figure 1. We assume that the vertical load is uniformly distributed and symmetric for the left and right main landing gears and that the suspension input signals of the left and right main landing gears are synchronized and symmetric. System parameters are illustrated in Table 1. According to Newton's second law, the dynamics of the full aircraft LGS can be described as

$$\begin{aligned}
M\ddot{z}_a &= -\big(k_{af}(z_{af}-z_f)+c_{af}(\dot{z}_{af}-\dot{z}_f)\big)-2\big(k_{am}(z_{am}-z_m)+c_{am}(\dot{z}_{am}-\dot{z}_m)\big)+u_f+2u_m,\\
M_f\ddot{z}_f &= \big(k_{af}(z_{af}-z_f)+c_{af}(\dot{z}_{af}-\dot{z}_f)\big)-\big(k_{fr}(z_f-z_{fr})+c_{fr}(\dot{z}_f-\dot{z}_{fr})\big)-u_f,\\
M_m\ddot{z}_m &= \big(k_{am}(z_{am}-z_m)+c_{am}(\dot{z}_{am}-\dot{z}_m)\big)-\big(k_{mr}(z_m-z_{mr})+c_{mr}(\dot{z}_m-\dot{z}_{mr})\big)-u_m,\\
I_\varphi\ddot{\varphi} &= \big(k_{af}(z_{af}-z_f)+c_{af}(\dot{z}_{af}-\dot{z}_f)\big)l_f-2\big(k_{am}(z_{am}-z_m)+c_{am}(\dot{z}_{am}-\dot{z}_m)\big)l_m-u_fl_f+2u_ml_m.
\end{aligned}\tag{1}$$

As the pitching angle of the aircraft fuselage is negligible in the actual process, i.e., $\sin\varphi\approx\varphi$, one has

$$\begin{aligned}
z_{af} &= z_a-l_f\sin\varphi\approx z_a-l_f\varphi,\\
z_{am} &= z_a+l_m\sin\varphi\approx z_a+l_m\varphi.
\end{aligned}\tag{2}$$

Let $x_1=z_{af}-z_f$, $x_2=z_f-z_{fr}$, $x_3=\dot{z}_{af}$, $x_4=\dot{z}_f$, $x_5=z_{am}-z_m$, $x_6=z_m-z_{mr}$, $x_7=\dot{z}_{am}$, $x_8=\dot{z}_m$, and define the state vectors of the front and main LGSs $x_f=[x_1\ x_2\ x_3\ x_4]^{\mathrm{T}}$, $x_m=[x_5\ x_6\ x_7\ x_8]^{\mathrm{T}}$,

Table 1 Parameters of aircraft LGS

Parameter	Description
x	Taxiing distance of aircraft fuselage
z_a	Vertical displacement of aircraft fuselage
φ	Pitching angle of aircraft fuselage
M	Mass of aircraft fuselage
M_f/M_m	Mass of front/main landing gear
g	Gravity acceleration
l_f/l_m	Horizontal distance from front/main landing gear to aircraft gravity
z_{af}/z_{am}	Vertical displacement of junction of aircraft fuselage and front/main landing gear
z_f/z_m	Vertical displacement of front/main landing gear
z_{fr}/z_{mr}	Runway excitations to front/main wheels
k_{af}/k_{am}	Stiffness of front/main active suspension
k_{fr}/k_{mr}	Stiffness of front/main wheels
c_{af}/c_{am}	Damping of front/main active suspension
c_{fr}/c_{mr}	Damping of front/main wheels
u_f/u_m	Control input of front/main active suspension

respectively, control input vector $u = [u_f \ u_m]^{\mathrm{T}}$, and measured outputs $y_f = x_1, y_m = x_5$. $\dot{z}_{fr}$ and $\dot{z}_{mr}$ are the irregular runway excitations to the front and main LGSs, respectively. Then, the mathematical models of the front and main LGSs are separately constructed as

$$\begin{cases} \dot{x}_f = A_f x_f + A_{fm} x_m + B_f u + D_f \dot{z}_{fr}, \\ y_f = C_f x_f, \end{cases} \tag{3a}$$

$$\begin{cases} \dot{x}_m = A_m x_m + A_{mf} x_f + B_m u + D_m \dot{z}_{mr}, \\ y_m = C_m x_m, \end{cases} \tag{3b}$$

where A_i, $i \in \{f, m\}$, are system matrices of the front and main LGSs, respectively, A_{ij}, $i, j \in \{f, m\}$, $i \neq j$, are coupled matrices of the front and main LGSs, respectively, and B_i, C_i, and D_i, $i \in \{f, m\}$, are control matrices, measured output matrices, and disturbance matrices of the front and main LGSs, respectively, which are given as follows:

$$A_f = \begin{bmatrix} 0 & 0 & 1 & -1 \\ 0 & 0 & 0 & 1 \\ -a_1 k_{af} & 0 & -a_1 c_{af} & a_1 c_{af} \\ a_4 k_{af} & -a_4 k_{fr} & a_4 c_{af} & -a_4(c_{af} + c_{fr}) \end{bmatrix}, \ B_f = \begin{bmatrix} 0 & 0 \\ 0 & 0 \\ a_1 & 2a_2 \\ -a_4 & 0 \end{bmatrix},$$

$$A_{fm} = \begin{bmatrix} 0 & 0 & 0 & 0 \\ 0 & 0 & 0 & 0 \\ -2a_2 k_{am} & 0 & -2a_2 c_{am} & 2a_2 c_{am} \\ 0 & 0 & 0 & 0 \end{bmatrix}, \ C_f = C_m = \begin{bmatrix} 1 \\ 0 \\ 0 \\ 0 \end{bmatrix},$$

$$A_m = \begin{bmatrix} 0 & 0 & 1 & -1 \\ 0 & 0 & 0 & 1 \\ -2a_3 k_{am} & 0 & -2a_3 c_{am} & 2a_3 c_{am} \\ a_5 k_{am} & -a_5 k_{mr} & a_5 c_{am} & -a_5(c_{am} + c_{mr}) \end{bmatrix}, \ B_m = \begin{bmatrix} 0 & 0 \\ 0 & 0 \\ a_2 & 2a_3 \\ 0 & -a_5 \end{bmatrix},$$

$$A_{mf} = \begin{bmatrix} 0 & 0 & 0 & 0 \\ 0 & 0 & 0 & 0 \\ -a_2 k_{af} & 0 & -a_2 c_{af} & a_2 c_{af} \\ 0 & 0 & 0 & 0 \end{bmatrix}, \ D_f = \begin{bmatrix} 0 \\ -1 \\ 0 \\ a_4 c_{fr} \end{bmatrix}, \ D_m = \begin{bmatrix} 0 \\ -1 \\ 0 \\ a_5 c_{mr} \end{bmatrix},$$

where $a_1 = \frac{1}{M} + \frac{l_f^2}{I_\varphi}$, $a_2 = \frac{1}{M} - \frac{l_f l_m}{I_\varphi}$, $a_3 = \frac{1}{M} + \frac{l_m^2}{I_\varphi}$, $a_4 = \frac{1}{M_f}$, $a_5 = \frac{1}{M_m}$, $a_6 = \frac{1}{M}$, $a_7 = \frac{l_f}{I_\varphi}$, and $a_8 = \frac{l_m}{I_\varphi}$.

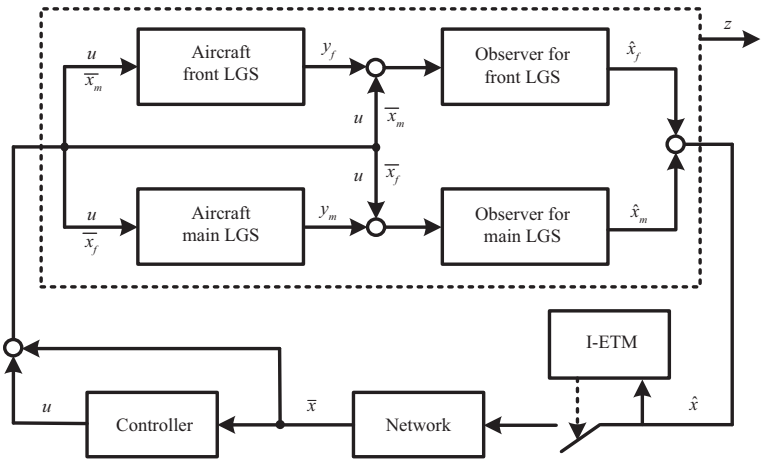

Figure 2 Overall networked control framework of the aircraft LGS.

To improve passenger safety and comfort, vibrations induced by landing impact and irregular runway excitations should be reduced; i.e., vertical acceleration and pitching angle acceleration of the fuselage should be as small as possible. Thus, the controlled output of the full aircraft LGS is defined as follows:

$$z = \begin{bmatrix} \ddot{z}_a \\ \ddot{\varphi} \end{bmatrix} = C_z \begin{bmatrix} x_f \\ x_m \end{bmatrix} + B_z u, \tag{4}$$

where

$$C_z = \begin{bmatrix} -a_6k_{af} & 0 & -a_6c_{af} & a_6c_{af} & -2a_6k_{am} & 0 & -2a_6c_{am} & 2a_6c_{am} \\ a_7k_{af} & 0 & a_7c_{af} & -a_7c_{af} & -2a_8k_{am} & 0 & -2a_8c_{am} & 2a_8c_{am} \end{bmatrix},$$
$$B_z = \begin{bmatrix} a_6 & 2a_6 \\ -a_7 & 2a_8 \end{bmatrix}.$$

Then, the full aircraft LGS is established and composed of (3a), (3b), and (4), and the objective of this article is to design an integrated active controller to stabilize the system and reduce the vibrations caused by landing impact and irregular runway excitations.

3 Construction of adaptive observers and integral ETM

In this section, two adaptive observers are designed to estimate the state of the front and main LGSs and identify the dampings of the gears and wheels, respectively. Subsequently, the estimated state is transmitted to the controller and LGSs over a shared network through the designed I-ETM; thus, the overall networked control framework of the full aircraft LGS is constructed.

As depicted in Figure 1, the control input signals generated by suspensions of the front and main LGSs are independent, but the suspension signal of one subsystem affects another subsystem, and information exchange between subsystems cannot be implemented directly. Furthermore, as presented in (3a) and (3b), only the variables $x_1 = z_{af} - z_f$ and $x_5 = z_{am} - z_m$ can be measured accurately for the front and main LGSs, respectively. Additionally, the damping parameters of landing gears and wheels, i.e., c_{af}, c_{am}, c_{fr}, and c_{mr}, vary during aircraft landing and taxiing processes. To overcome these problems, two adaptive observers are designed separately for the front and main LGSs, respectively, to identify the damping parameters and estimate the states of LGSs simultaneously. Subsequently, the estimated states are transmitted to the controller and subsystems over a shared network through the novel I-ETM, the information exchange between them is realized, and the front and main subsystems are interconnected. Thus, the overall networked control framework of the full aircraft LGS is constructed in Figure 2.

The front and main LGSs with the transmitted signals, i.e., $\bar{x}_m$ and $\bar{x}_f$, and the designed adaptive

observers are described as

$$\begin{cases} \dot{x}_f = A_f x_f + A_{fm}\bar{x}_m + B_f u + D_f \dot{z}_{fr}, \\ y_f = C_f x_f, \\ \dot{\hat{x}}_f = \hat{A}_f \hat{x}_f + \hat{A}_{fm}\bar{x}_m + B_f u + L_f(y_f - C_f \hat{x}_f), \end{cases} \tag{5a}$$

$$\begin{cases} \dot{x}_m = A_m x_m + A_{mf}\bar{x}_f + B_m u + D_m \dot{z}_{mr}, \\ y_m = C_m x_m, \\ \dot{\hat{x}}_m = \hat{A}_m \hat{x}_m + \hat{A}_{mf}\bar{x}_f + B_m u + L_m(y_m - C_m \hat{x}_m), \end{cases} \tag{5b}$$

for $t \in [t_k, t_{k+1})$, and t_k, $k \in \mathbb{Z}_{\geqslant 0}$, is the transmission time instant determined by the integral event-triggered mechanism, where L_f, L_m with appropriate dimensions are gain matrices of observers for the front and main LGSs, respectively, which will be designed later. Moreover, $\bar{x}_f(t) = \hat{x}_f(t_k)$, $\bar{x}_m(t) = \hat{x}_m(t_k)$ for $t \in [t_k, t_{k+1})$, $k \in \mathbb{Z}_{\geqslant 0}$, are the state signals of the adaptive observers transmitting to the shared network, and the controller and both subsystems can receive the transmitted signals at time instants t_k, $k \in \mathbb{Z}_{\geqslant 0}$. Otherwise, the transmitted signals will be kept constant between two successive transmission instants by zero-order holders. Thus, we have $\dot{\bar{x}}_f(t) = \dot{\bar{x}}_m(t) = 0$ for $t \in [t_k, t_{k+1})$, $\bar{x}_f(t_k^+) = \hat{x}_f(t_k)$, $\bar{x}_m(t_k^+) = \hat{x}_m(t_k)$ for $k \in \mathbb{Z}_{\geqslant 0}$. We introduce a timer $\tau := t - t_k \in \mathbb{R}_{\geqslant 0}$ to describe the elapsed time since the last transmission instant, and we obtain $\dot{\tau} = 1$ for $t \in [t_k, t_{k+1})$, $\tau(t_k^+) = 0$, $k \in \mathbb{Z}_{\geqslant 0}$. Define the estimated state errors $\tilde{x}_f = \hat{x}_f - x_f$, $\tilde{x}_m = \hat{x}_m - x_m$, the identified damping errors $\phi_f = [\hat{c}_{af} - c_{af}\ \hat{c}_{fr} - c_{fr}]^{\mathrm{T}}$, $\phi_m = [\hat{c}_{am} - c_{am}\ \hat{c}_{mr} - c_{mr}]^{\mathrm{T}}$, network induced errors $e_f = \bar{x}_f - \hat{x}_f$, $e_m = \bar{x}_m - \hat{x}_m$ for $t \in [t_k, t_{k+1})$, $k \in \mathbb{Z}_{\geqslant 0}$, and let $x = [x_f^{\mathrm{T}}\ x_m^{\mathrm{T}}]^{\mathrm{T}}$, $\hat{x} = [\hat{x}_f^{\mathrm{T}}\ \hat{x}_m^{\mathrm{T}}]^{\mathrm{T}}$, $\bar{x} = [\bar{x}_f^{\mathrm{T}}\ \bar{x}_m^{\mathrm{T}}]^{\mathrm{T}}$, $\tilde{x} = [\tilde{x}_f^{\mathrm{T}}\ \tilde{x}_m^{\mathrm{T}}]^{\mathrm{T}}$, $\phi = [\phi_f^{\mathrm{T}}\ \phi_m^{\mathrm{T}}]^{\mathrm{T}}$, $e = [e_f^{\mathrm{T}}\ e_m^{\mathrm{T}}]^{\mathrm{T}}$, $d = [\dot{z}_{fr}\ \dot{z}_{mr}]^{\mathrm{T}}$.

Subsequently, the integrated active controller is synthesized on the basis of the transmitted signals as

$$u = \begin{bmatrix} u_f \\ u_m \end{bmatrix} = \begin{bmatrix} K_f \bar{x}_f \\ K_m \bar{x}_m \end{bmatrix} = K\bar{x}, \tag{6}$$

where the controller gain matrix $K := \left[\begin{smallmatrix} K_f & O \\ O & K_m \end{smallmatrix}\right]$, and $K_f, K_m \in \mathbb{R}^{1\times 4}$ will be designed later.

The novel I-ETM for signal transmission is designed as follows:

$$t_{k+1} = \inf\{(t - t_k \geqslant T \mid \eta \leqslant 0) \text{ or } (t - t_k \geqslant \mathcal{T})\} \tag{7}$$

with $t_0 = 0$, $k \in \mathbb{Z}_{\geqslant 0}$. T and $\mathcal{T}$ are the lower and upper bounds of the interevent time of the I-ETM, and T is used to avoid the Zeno phenomenon and determined by

$$T(r) = \begin{cases} \frac{1}{Gl}\arctan\frac{l(1-r)}{\frac{2\zeta r}{G(1+r)} + \frac{r^2+1}{r+1}}, & \zeta > G, \\ \frac{1-r}{G(1+r)}, & \zeta = G, \\ \frac{1}{Gl}\operatorname{arctanh}\frac{l(1-r)}{\frac{2\zeta r}{G(1+r)} + \frac{r^2+1}{r+1}}, & \zeta < G, \end{cases} \tag{8}$$

where $r \in (0,1)$, $l = \sqrt{|(\frac{\zeta}{G})^2 - 1|}$, ζ is a given scalar, G is determined by (14) in Definition 2, which will be illustrated in the following text, and $\mathcal{T}$ is limited by actual applications.

Additionally, the internal variable η in (7) is calculated as follows:

$$\eta(t) = \int_{t_k}^{t} \varepsilon \hat{x}^{\mathrm{T}}(s)\hat{x}(s) - (1 - \beta(\tau(s)))\alpha(\tau(s))W^2(e(s))\mathrm{d}s \tag{9}$$

with $\eta(t_k^+) = 0$, where $W(e) := \lambda\|e\|$ is defined satisfying (13) and (14). In Definition 2, λ and ε are given positive scalars, $\beta(\tau) = 1$ for $0 \leqslant \tau < T$, $\beta(\tau) = 0$ for $T \leqslant \tau \leqslant \mathcal{T}$, and $\alpha(\tau) = \zeta(2\varpi(\tau)G + \zeta(1 + \varpi^2(\tau)))$. The function $\varpi(\tau) : \mathbb{R}_{\geqslant 0} \to \mathbb{R}$ is described as follows:

$$\frac{\mathrm{d}\varpi(\tau)}{\mathrm{d}\tau} = \begin{cases} -2G\varpi(\tau) - \zeta(\varpi^2(\tau) + 1), & 0 \leqslant \tau < T, \\ 0, & T \leqslant \tau \leqslant \mathcal{T}, \end{cases} \tag{10}$$

with $\varpi(0) = r^{-1}$, $\varpi(\tau) = r$ for $\tau \geqslant T$.

Let $\hbar := \dot{\eta} = \varepsilon \hat{x}^{\mathrm{T}} \hat{x} - (1-\beta)\alpha W^2$ and $q := [\hat{x}^{\mathrm{T}}\ \tilde{x}^{\mathrm{T}}\ e^{\mathrm{T}}\ \phi^{\mathrm{T}}\ \eta\ \tau]^{\mathrm{T}}$. Then, according to (5a), (5b), (6), and (9) with an adaptive law that will be synthesized in Theorem 1 later, the resulting hybrid system is characterized as

$$\begin{aligned} \dot{q} &= \begin{pmatrix} (\mathcal{A}_1 + \mathcal{A}_2 + \mathcal{B}K)\hat{x} - \mathcal{L}_c\tilde{x} + (\mathcal{A}_2 + \mathcal{B}K)e + \mathcal{M}\phi \\ (\mathcal{A}_1 - \mathcal{L}_c)\tilde{x} + \mathcal{M}\phi - \mathcal{D}d \\ -(\mathcal{A}_1 + \mathcal{A}_2 + \mathcal{B}K)\hat{x} + \mathcal{L}_c\tilde{x} - (\mathcal{A}_2 + \mathcal{B}K)e - \mathcal{M}\phi \\ \dot{\phi} \\ \hbar \\ 1 \end{pmatrix}, \ q \in \mathcal{F}, \\ q^+ &\in \{(\hat{x}, \tilde{x}, 0, \phi, 0, 0)\}, \qquad q \in \mathcal{J}, \end{aligned} \tag{11}$$

with the flow and jump sets

$$\begin{aligned} \mathcal{F} &= \{q | (\eta \geqslant 0) \vee (\tau < T)\}, \\ \mathcal{J} &= \{q | ((\eta \leqslant 0) \wedge (\tau \geqslant T)) \vee (\tau \geqslant \mathcal{T})\}, \end{aligned} \tag{12}$$

where

$$\begin{aligned} &\mathcal{A}_1 = \begin{bmatrix} A_f & 0 \\ 0 & A_m \end{bmatrix}, \ \mathcal{A}_2 = \begin{bmatrix} 0 & A_{fm} \\ A_{mf} & 0 \end{bmatrix}, \ \mathcal{B} = \begin{bmatrix} B_f \\ B_m \end{bmatrix}, \ \mathcal{D} = \begin{bmatrix} D_f & 0 \\ 0 & D_m \end{bmatrix}, \\ &\mathcal{L}_c = \begin{bmatrix} L_f C_f & 0 \\ 0 & L_m C_m \end{bmatrix}, \ \mathcal{M} = \begin{bmatrix} \mathcal{M}_f & \mathcal{M}_{fm} \\ \mathcal{M}_{mf} & \mathcal{M}_m \end{bmatrix}, \ \mathcal{M}_f = \begin{bmatrix} M_1\hat{x}_f \\ M_2\hat{x}_f \end{bmatrix}, \\ &\mathcal{M}_{fm} = \begin{bmatrix} M_3(\hat{x}_m + e_m) \\ O \end{bmatrix}, \ \mathcal{M}_m = \begin{bmatrix} M_4\hat{x}_m \\ M_5\hat{x}_m \end{bmatrix}, \ \mathcal{M}_{mf} = \begin{bmatrix} M_6(\hat{x}_f + e_f) \\ O \end{bmatrix}, \\ &M_1 = \begin{bmatrix} 0 & 0 & 0 & 0 \\ 0 & 0 & 0 & 0 \\ 0 & 0 & -a_1 & a_1 \\ 0 & 0 & a_4 & -a_4 \end{bmatrix}, \ M_2 = \begin{bmatrix} 0 & 0 & 0 & 0 \\ 0 & 0 & 0 & 0 \\ 0 & 0 & 0 & 0 \\ 0 & 0 & 0 & -a_4 \end{bmatrix}, \ M_3 = \begin{bmatrix} 0 & 0 & 0 & 0 \\ 0 & 0 & 0 & 0 \\ 0 & 0 & -2a_2 & 2a_2 \\ 0 & 0 & 0 & 0 \end{bmatrix}, \\ &M_4 = \begin{bmatrix} 0 & 0 & 0 & 0 \\ 0 & 0 & 0 & 0 \\ 0 & 0 & -2a_3 & 2a_3 \\ 0 & 0 & a_5 & -a_5 \end{bmatrix}, \ M_5 = \begin{bmatrix} 0 & 0 & 0 & 0 \\ 0 & 0 & 0 & 0 \\ 0 & 0 & 0 & 0 \\ 0 & 0 & 0 & -a_5 \end{bmatrix}, \ M_6 = \begin{bmatrix} 0 & 0 & 0 & 0 \\ 0 & 0 & 0 & 0 \\ 0 & 0 & -a_2 & a_2 \\ 0 & 0 & 0 & 0 \end{bmatrix}. \end{aligned}$$

For simplicity, we define $\dot{q} := F(q, d)$ and $q^+ \in J(q)$ in the following text.

Remark 1. The networked control framework of the aircraft LGS is developed to implement the information exchange between the front and main subsystems over a shared network. Thus, more state information could be accessible to the subsystems and controller by the designed observers because only a single variable can be measured accurately for the original subsystem. Furthermore, control input signals are generated independently for the front and main suspensions, but they interact with each other. The joint design of the active controller, instead of designing controllers for each subsystem separately, fully considers the interconnection of subsystems, consequently improving the robustness against the pitching vibration of the aircraft.

The following definitions and assumptions are recalled for the hybrid system (11) with flow and jump sets (12) and controlled output (4).

Definition 1 ([23])**.** For a hybrid signal z defined on the hybrid time domain $\mathrm{dom}\, z = \cup_{k=0}^{K-1}[t_k, t_{k+1}] \times \{k\}$ with K possibly ∞ or $t_K = \infty$, the $\mathcal{L}_2$-norm of z is defined as $\|z\|_2 := \big(\sum_{k=0}^{K-1} \int_{t_k}^{t_{k+1}} \|z(t,k)\|^2 \mathrm{d}t\big)^{\frac{1}{2}}$, provided that the right-hand side exists and is finite, in which case we write $z \in \mathcal{L}_2$.

Assumption 1. It is assumed that the irregular runway excitations $\dot{z}_{fr}, \dot{z}_{mr}$ exist and belong to $\mathcal{L}_2$.

Definition 2 ([23])**.** The hybrid system (11) with flow and jump sets (12) is said to be $\mathcal{L}_2$-stable from the input $d \in \mathcal{L}_2$ to the controlled output in z (4) with gain less than or equal to $\vartheta \geqslant 0$, if there exist positive definite function $W : \mathbb{R}^8 \to \mathbb{R}_{\geqslant 0}$, a locally Lipschitz function $V : \mathbb{R}^{8+8+4} \to \mathbb{R}_{\geqslant 0}$, $\mathcal{K}_\infty$-functions $\underline{\chi}_W$, $\overline{\chi}_W : \mathbb{R}^8 \to \mathbb{R}_{\geqslant 0}$, $\underline{\chi}_V$, $\overline{\chi}_V : \mathbb{R}^{8+8+4} \to \mathbb{R}_{\geqslant 0}$, $\chi_\Upsilon : \mathbb{R}^{8+8+8+4+1} \to \mathbb{R}_{\geqslant 0}$, positive semi-definite function $\rho : \mathbb{R}^8 \to \mathbb{R}_{\geqslant 0}$, continuous function $H : \mathbb{R}^{8+8+4+2} \to \mathbb{R}_{\geqslant 0}$, real number $G \geqslant 0$ such that

(1) for all e it holds that

$$\underline{\chi}_W(\|e\|) \leqslant W(e) \leqslant \overline{\chi}_W(\|e\|); \tag{13}$$

(2) for all $\hat{x}, \tilde{x}, \phi, d$ and almost all e it holds that

$$\dot{W} \leqslant GW(e) + H(\hat{x}, \tilde{x}, \phi, d); \tag{14}$$

(3) for all $\hat{x}, \tilde{x}, \phi$ it holds that

$$\underline{\chi}_V(\|(\hat{x}, \tilde{x}, \phi)\|) \leqslant V(\hat{x}, \tilde{x}, \phi) \leqslant \overline{\chi}_V(\|(\hat{x}, \tilde{x}, \phi)\|); \tag{15}$$

(4) for all e, d and almost all $\hat{x}, \tilde{x}, \phi$ it holds that

$$\dot{V}(\hat{x}, \tilde{x}, \phi) \leqslant \zeta^2 W^2(e) - H^2(\hat{x}, \tilde{x}, \phi, d) - \rho(\hat{x}) + \vartheta^2 \|d\|^2 - \|z\|^2; \tag{16}$$

(5) for any solution pair $(\hat{x}, \tilde{x}, e, \phi, \eta)$ to the hybrid system (11) it satisfies that

$$\|z\|_2 \leqslant \vartheta \|d\|_2 + \chi_\Upsilon(\|(\hat{x}(0,0), \tilde{x}(0,0), e(0,0), \phi(0), \eta(0,0))\|). \tag{17}$$

Remark 2. As shown in (9), the variable η increases when $\tau \in [0, T]$ with $\beta(\tau) = 1$, increases constantly in the early stage of $\tau \geqslant T$, and starts decreasing only when the condition $\varepsilon \hat{x}^{\mathrm{T}} \hat{x} \geqslant \alpha(\tau) W^2(e)$ is violated with $\beta(\tau) = 0$. Thus, the I-ETM designed in (7) is triggered only when η drops to zero or the elapsed time since the last transmission instant exceeds the upper bound of the interevent time, i.e., $\tau \geqslant \mathcal{T}$. This result indicates that the proposed I-ETM will not be triggered during the early stage of $\tau \geqslant T$, even when $\varepsilon \hat{x}^{\mathrm{T}} \hat{x} \leqslant \alpha(\tau) W^2(e)$ under the condition $\eta > 0$. However, the S-ETMs in [22] will be activated once the condition $\varepsilon \hat{x}^{\mathrm{T}} \hat{x} \leqslant \alpha(\tau) W^2(e)$, $\|e\| \geqslant \varepsilon$ or $\varepsilon |\hat{x}| \leqslant \zeta |e|$ is reached. Thus, the duration between two successive transmission instants of the proposed I-ETM will be larger than that of traditional S-ETMs at the same initial triggering instant and state. Therefore, the signal transmission frequency of the proposed I-ETM will be substantially reduced, and more network communication resources can be saved.

4 Main results

In this section, an adaptive law is first developed to identify the damping parameters of the gears and wheels, and then a sufficient condition is given to guarantee the $\mathcal{L}_2$-stability of the hybrid system. Furthermore, feasible solutions for the gain matrices of the controller and observers are presented.

Theorem 1. Considering the hybrid system (11) with flow and jump sets (12), given scalars $\lambda \in (0, 1)$, $\zeta > 0$, $\zeta_\phi > 0$, if there exist positive scalars ε, ϑ and matrices $P > 0$, $\mathcal{L}_c$, K with appropriate dimensions such that the following inequality:

$$\Omega = \begin{bmatrix} \Omega_{1,1} & \Omega_{1,2} & \Omega_{1,3} & 0 \\ * & \Omega_{2,2} & -C_z^{\mathrm{T}} B_z K & -P\mathcal{D}^{\mathrm{T}} \\ * & * & \Omega_{3,3} & 0 \\ * & * & * & -\vartheta^2 I_2 \end{bmatrix} < 0 \tag{18}$$

holds, where

$$\begin{aligned} \Omega_{1,1} &= P(\mathcal{A}_1 + \mathcal{A}_2 + \mathcal{B}K) + (\mathcal{A}_1 + \mathcal{A}_2 + \mathcal{B}K)^{\mathrm{T}} P + (C_z + B_z K)^{\mathrm{T}} (C_z + B_z K) \\ &\quad + \lambda^2 (\mathcal{A}_1 + \mathcal{A}_2 + \mathcal{B}K)^{\mathrm{T}} (\mathcal{A}_1 + \mathcal{A}_2 + \mathcal{B}K) + \varepsilon I_8, \\ \Omega_{1,2} &= -P\mathcal{L}_c - \lambda^2 (\mathcal{A}_1 + \mathcal{A}_2 + \mathcal{B}K)^{\mathrm{T}} \mathcal{L}_c - (C_z + B_z K)^{\mathrm{T}} C_z, \end{aligned}$$

$$\begin{aligned}\Omega_{1,3} &= P(\mathcal{A}_2+\mathcal{B}K)+(C_z+B_zK)^{\mathrm{T}}B_zK,\\ \Omega_{2,2} &= P(\mathcal{A}_1-\mathcal{L}_c)+(\mathcal{A}_1-\mathcal{L}_c)^{\mathrm{T}}P+\lambda^2\mathcal{L}_c^{\mathrm{T}}\mathcal{L}_c+C_z^{\mathrm{T}}C_z,\\ \Omega_{3,3} &= K^{\mathrm{T}}B_z^{\mathrm{T}}B_zK-\zeta^2\lambda^2I_8,\end{aligned}$$

then, the closed-loop system with the adaptive law synthesized as

$$\dot{\phi} = -\zeta_\phi\mathcal{M}^{\mathrm{T}}\left((P+\lambda^2(\mathcal{A}_1+\mathcal{A}_2+\mathcal{B}K))\hat{x}+(P-\lambda^2\mathcal{L}_c)\tilde{x}+\frac{1}{2}\lambda^2\mathcal{M}\phi\right) \tag{19}$$

is $\mathcal{L}_2$-stable with the $\mathcal{L}_2$-gain less than or equal to ϑ.

Proof. Choose a candidate Lyapunov function

$$\Upsilon(q) = V(\hat{x},\tilde{x},\phi)+\zeta\varpi(\tau)W^2(e)+\eta \tag{20}$$

with $V(\hat{x},\tilde{x},\phi)=\hat{x}^{\mathrm{T}}P\hat{x}+\tilde{x}^{\mathrm{T}}P\tilde{x}+\frac{1}{\zeta_\phi}\phi^{\mathrm{T}}\phi$, where $P>0$ and ζ_ϕ is a given positive scalar.

It follows from (7) and (10) that $\eta\geqslant 0$ and $\varpi(\tau)\in[r,r^{-1}]$, $r\in(0,1)$; then, $\Upsilon(q)\geqslant 0$ always holds. In addition, the derivative of the Lyapunov function $\Upsilon(q)$ along with (11) is given by

$$\langle\Upsilon(q),F(q,d)\rangle \leqslant \dot{V}+\varepsilon\hat{x}^{\mathrm{T}}\hat{x}+2\zeta\varpi W(GW+H)+\zeta W^2\dot{\varpi}-(1-\beta)\alpha W^2. \tag{21}$$

For $0\leqslant\tau<T$, we obtain $\dot{\varpi}=-2G\varpi-\zeta(\varpi^2+1)$ with $\beta=1$, which implies that

$$\begin{aligned}\langle\Upsilon(q),F(q,d)\rangle &\leqslant \dot{V}+\varepsilon\hat{x}^{\mathrm{T}}\hat{x}+2\zeta\varpi WH-\zeta^2\varpi^2W^2-\zeta^2W^2\\ &\leqslant \dot{V}+\varepsilon\hat{x}^{\mathrm{T}}\hat{x}+H^2-\zeta^2W^2.\end{aligned} \tag{22}$$

For $T\leqslant\tau\leqslant\mathcal{T}$, we have $\dot{\varpi}=0$ with $\beta=0$, and the inequality (22) holds as well.

Choose $H(\hat{x},\tilde{x},\phi,d)=\lambda\|(\mathcal{A}_1+\mathcal{A}_2+\mathcal{B}K)\hat{x}-\mathcal{L}_c\tilde{x}+\mathcal{M}\phi\|$ and $G=\|\mathcal{A}_2+\mathcal{B}K\|$ such that the condition (14) in Definition 2 is satisfied. Then, taking the $\mathcal{L}_2$ index into account, it follows from (4), (11), and (19) that

$$\begin{aligned}&\langle\Upsilon(q),F(q,d)\rangle+\|z\|^2-\vartheta^2\|d\|^2\\ &\quad\leqslant \dot{V}+\varepsilon\hat{x}^{\mathrm{T}}\hat{x}+H^2-\zeta^2W^2+\|z\|^2-\vartheta^2\|d\|^2\\ &\quad= 2\hat{x}^{\mathrm{T}}P\big((\mathcal{A}_1+\mathcal{A}_2+\mathcal{B}K)\hat{x}-\mathcal{L}_c\tilde{x}+(\mathcal{A}_2+\mathcal{B}K)e+\mathcal{M}\phi\big)\\ &\qquad+2\tilde{x}^{\mathrm{T}}P\big((\mathcal{A}_1-\mathcal{L}_c)\tilde{x}+\mathcal{M}\phi-\mathcal{D}d\big)+2\frac{1}{\zeta_\phi}\phi^{\mathrm{T}}\dot{\phi}\\ &\qquad+\varepsilon\hat{x}^{\mathrm{T}}\hat{x}+\lambda^2\hat{x}^{\mathrm{T}}(\mathcal{A}_1+\mathcal{A}_2+\mathcal{B}K)^{\mathrm{T}}(\mathcal{A}_1+\mathcal{A}_2+\mathcal{B}K)\hat{x}\\ &\qquad-2\lambda^2\hat{x}^{\mathrm{T}}(\mathcal{A}_1+\mathcal{A}_2+\mathcal{B}K)^{\mathrm{T}}\mathcal{L}_c\tilde{x}+2\lambda^2\hat{x}^{\mathrm{T}}(\mathcal{A}_1+\mathcal{A}_2+\mathcal{B}K)^{\mathrm{T}}\mathcal{M}\phi\\ &\qquad+\lambda^2\tilde{x}^{\mathrm{T}}\mathcal{L}_c^{\mathrm{T}}\mathcal{L}_c\tilde{x}-2\lambda^2\tilde{x}^{\mathrm{T}}\mathcal{L}_c^{\mathrm{T}}\mathcal{M}\phi+\lambda^2\phi^{\mathrm{T}}\mathcal{M}^{\mathrm{T}}\mathcal{M}\phi-\lambda^2\zeta^2e^{\mathrm{T}}e\\ &\qquad+\hat{x}^{\mathrm{T}}(C_z+B_zK)^{\mathrm{T}}(C_z+B_zK)\hat{x}+\tilde{x}^{\mathrm{T}}C_z^{\mathrm{T}}C_z\tilde{x}+e^{\mathrm{T}}\\ &\qquad-2\hat{x}^{\mathrm{T}}(C_z+B_zK)^{\mathrm{T}}C_z\tilde{x}+2\hat{x}^{\mathrm{T}}(C_z+B_zK)^{\mathrm{T}}B_zKe\\ &\qquad+2\tilde{x}^{\mathrm{T}}C_z^{\mathrm{T}}B_zKe-\vartheta^2d^{\mathrm{T}}d.\end{aligned} \tag{23}$$

Defining a variable vector $\xi=[\hat{x}^{\mathrm{T}}\ \tilde{x}^{\mathrm{T}}\ e^{\mathrm{T}}\ d^{\mathrm{T}}]^{\mathrm{T}}$, using the adaptive law (19), one can obtain

$$\langle\Upsilon(q),F(q,d)\rangle+\|z\|^2-\vartheta^2\|d\|^2\leqslant\xi^{\mathrm{T}}\Omega\xi. \tag{24}$$

If the condition (18) in Theorem 1 is satisfied, we find that $\dot{V}+\varepsilon\hat{x}^{\mathrm{T}}\hat{x}+H^2-\zeta^2W^2+\|z\|^2-\vartheta^2\|d\|^2\leqslant 0$ holds, which is equivalent to (16) in Definition 2 with $\rho(\hat{x})=\varepsilon\hat{x}^{\mathrm{T}}\hat{x}$. Moreover, we find that

$$\langle\Upsilon(q),F(q,d)\rangle \leqslant \vartheta^2\|d\|^2-\|z\|^2. \tag{25}$$

Furthermore, when there is a jump, i.e., $q\in\mathcal{J}$, we have $e(t_k^+)=0$, $\eta(t_k^+)=0$, $\tau\geqslant T$, and $\varpi(\tau)=r$. Consequently, $\Upsilon(q(t_k^+))-\Upsilon(q(t_k))=-\zeta rW^2(e(t_k))-\eta(t_k)\leqslant 0$ holds for $k\in\mathbb{Z}_{\geqslant 0}$, indicating that $\Upsilon(q(t_{k+1},k+1))-\Upsilon(q(t_{k+1},k))\leqslant 0$ holds. Then, integrating (25), one can get that

$$\|z\|_2^2=\sum_{k=0}^{K-1}\int_{t_k}^{t_{k+1}}\|z(t,k)\|^2\mathrm{d}t$$

$$
\begin{aligned}
&\leqslant \sum_{k=0}^{K-1}\left[\vartheta^2\int_{t_k}^{t_{k+1}}\|d(t,k)\|^2\mathrm{d}t-(\Upsilon(q(t_{k+1},k))-\Upsilon(q(t_k,k)))\right]\\
&=\vartheta^2\|d\|_2^2+\Upsilon(q(t_0,0))-\Upsilon(q(t_K,K-1))+\sum_{k=0}^{K-2}(\Upsilon(q(t_{k+1},k+1))-\Upsilon(q(t_{k+1},k)))\\
&\leqslant \vartheta^2\|d\|_2^2+\Upsilon(q(0,0))\\
&\leqslant \left(\vartheta\|d\|_2+\Upsilon(q(0,0))^{\frac{1}{2}}\right)^2. \qquad (26)
\end{aligned}
$$

Because the Lyapunov function $\Upsilon(q)$ is bounded, there exists a $\mathcal{K}_\infty$-function $\varrho_\Upsilon(\|(\hat{x},\tilde{x},e,\phi,\eta)\|)$ such that $\Upsilon(q)^{\frac{1}{2}}\leqslant\varrho_\Upsilon(\|(\hat{x},\tilde{x},e,\phi,\eta)\|)$. Subsequently, we easily find that

$$
\|z\|_2\leqslant\vartheta\|d\|_2+\Upsilon(q(0,0))^{\frac{1}{2}}\leqslant\vartheta\|d\|_2+\varrho_\Upsilon(\|(\hat{x}(0,0),\tilde{x}(0,0),e(0,0),\phi(0),\eta(0,0))\|)
$$

holds. This completes the proof.

Theorem 2. Considering the hybrid system (11) with flow and jump sets (12), the adaptive law is synthesized as (19). Given scalars $\lambda\in(0,1)$, $\zeta>0$, and $\zeta_\phi>0$, if there exist positive scalars $\bar{\varepsilon}$ and $\bar{\vartheta}$, and matrices $\mathcal{P}=\mathrm{diag}\{\mathcal{P}_f,\mathcal{P}_m\}$ with $\mathcal{P}_i\in\mathbb{R}^{4\times4}>0$, $i\in\{f,m\}$, $\mathcal{K}=\mathrm{diag}\{\mathcal{K}_f,\mathcal{K}_m\}$ with $\mathcal{K}_i\in\mathbb{R}^{1\times4}$, and $\mathcal{L}_P=\mathrm{diag}\{\mathcal{L}_{Pf},\mathcal{L}_{Pm}\}$ with $\mathcal{L}_{Pi}\in\mathbb{R}^{4\times4}$ such that the following inequality:

$$
\tilde{\Omega}=\begin{bmatrix}
\tilde{\Omega}_{1,1} & -\mathcal{L}_P & \tilde{\Omega}_{1,3} & 0 & \tilde{\Omega}_{1,5} & \tilde{\Omega}_{1,6} & \mathcal{P}\\
* & \tilde{\Omega}_{2,2} & 0 & -\mathcal{D}^{\mathrm{T}} & -\lambda\mathcal{L}_P^{\mathrm{T}} & -\mathcal{P}C_z^{\mathrm{T}} & 0\\
* & * & \tilde{\Omega}_{3,3} & 0 & 0 & 0 & 0\\
* & * & * & -\bar{\vartheta}I_2 & 0 & 0 & 0\\
* & * & * & * & -I_8 & 0 & 0\\
* & * & * & * & * & -I_2 & 0\\
* & * & * & * & * & * & -\bar{\varepsilon}I_8
\end{bmatrix}<0 \qquad (27)
$$

holds, where

$$
\begin{aligned}
\tilde{\Omega}_{1,1}&=(\mathcal{A}_1+\mathcal{A}_2)\mathcal{P}+\mathcal{P}(\mathcal{A}_1+\mathcal{A}_2)^{\mathrm{T}}+\mathcal{B}\mathcal{K}+\mathcal{K}^{\mathrm{T}}\mathcal{B}^{\mathrm{T}},\\
\tilde{\Omega}_{1,3}&=\mathcal{A}_2\mathcal{P}+\mathcal{B}\mathcal{K},\\
\tilde{\Omega}_{1,5}&=\lambda\mathcal{P}(\mathcal{A}_1+\mathcal{A}_2)^{\mathrm{T}}+\lambda\mathcal{K}^{\mathrm{T}}\mathcal{B}^{\mathrm{T}},\\
\tilde{\Omega}_{1,6}&=\mathcal{P}C_z^{\mathrm{T}}+\mathcal{K}^{\mathrm{T}}\mathcal{B}_z^{\mathrm{T}},\\
\tilde{\Omega}_{2,2}&=\mathcal{A}_1\mathcal{P}+\mathcal{P}\mathcal{A}_1^{\mathrm{T}}-\mathcal{L}_P-\mathcal{L}_P^{\mathrm{T}},\\
\tilde{\Omega}_{3,3}&=-\lambda^2\zeta^2(\mathcal{P}+\mathcal{P}^{\mathrm{T}}-I_8),
\end{aligned}
$$

then, the closed-loop system is $\mathcal{L}_2$-stable from d to z with the $\mathcal{L}_2$-gain less than or equal to ϑ, and the gain matrices of the controller and observers are given by $K=\mathcal{K}\mathcal{P}^{-1}$, $L_f=\mathcal{L}_{Pf}\mathcal{P}_f^{-1}C_f^{\mathrm{T}}$, and $L_m=\mathcal{L}_{Pm}\mathcal{P}_m^{-1}C_m^{\mathrm{T}}$.

Proof. Let $\mathcal{P}=P^{-1}>0$ by multiplying to the left of (18) by the diagonal matrix $\mathrm{diag}\{\mathcal{P},\mathcal{P},\mathcal{P},I\}$ and to the right by its transpose, respectively. Then, by using $\mathcal{K}=K\mathcal{P}$, $\mathcal{L}_P=\mathcal{L}_c\mathcal{P}$, $\bar{\varepsilon}=\varepsilon^{-1}$, $\bar{\vartheta}=\vartheta^2$, and Schur complement with $\mathcal{P}+\mathcal{P}^{\mathrm{T}}-I\leqslant\mathcal{P}^{\mathrm{T}}\mathcal{P}$, one can easily get that Eq. (27) holds. This completes the proof.

5 Simulation results

In this section, we present the simulation results to demonstrate the effectiveness and superiority of the adaptive observer-based integral event-triggered active antivibration control method for the full aircraft LGS. The parameters of the full aircraft LGS are given as follows: $M=22000$ kg, $M_f=130$ kg, $M_m=260$ kg, $l_f=3.76$ m, $l_m=1.94$ m, $I_\varphi=165000$ kg$\cdot$m^2, $k_{af}=673000$ N/m, $k_{am}=408000$ N/m, $k_{fr}=1590000$ N/m, $k_{mr}=1590000$ N/m. Damping parameters of the front and main landing gears

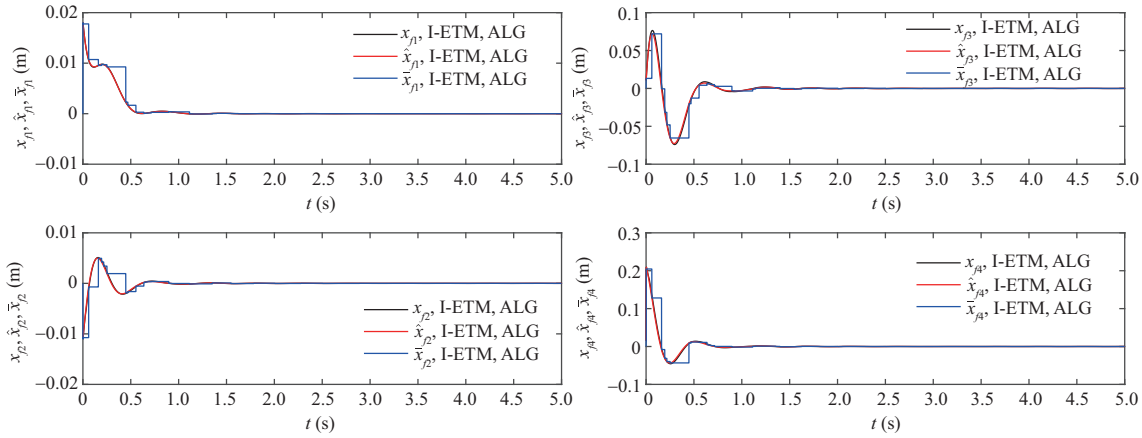

Figure 3 (Color online) Actual, estimated, and transmitted states of the front LGS.

and wheels vary during the aircraft landing process and are expressed as follows: $c_{af} = 143000 + 20000\sin(0.4t)$ N · s/m, $c_{am} = 625000 + 20000\sin(0.4t)$ N · s/m, $c_{fr} = 4060 - 1000\sin(0.2t)$ N · s/m, $c_{mr} = 4060 - 1000\sin(0.2t)$ N · s/m. The design parameters are given as follows: $\lambda = 2.02 \times 10^{-3}$, $\zeta = 6.25 \times 10^2$, $r = 0.1$, $\zeta_\phi = 0.5$. By solving the condition (27) in Theorem 2 with $\vartheta = 3.8416$ and $\varepsilon = 0.4059$, one can get the gain matrices of the controller and observers for the front and main LGSs:

$$K_f = \begin{bmatrix} -1003.2684 & -759.6426 & -3046.8200 & 69.9476 \end{bmatrix},$$
$$K_m = \begin{bmatrix} -1303.1356 & -469.0160 & -3154.6903 & 1596.1660 \end{bmatrix},$$
$$L_f = \begin{bmatrix} 28.2801 & -14.1555 & -51.1780 & 758.9099 \end{bmatrix}^{\mathrm{T}},$$
$$L_m = \begin{bmatrix} 17.4620 & -25.2652 & 4.9164 & -745.8878 \end{bmatrix}^{\mathrm{T}}.$$

The simulation time is 5 s, the sampling time is 5×10^{-4} s, and the initial states of the front and main LGSs are $x_f(0,0,0,0) = [0.018\ -0.011\ 0.012\ 0.015]^{\mathrm{T}}$, $x_m(0,0,0,0) = [-0.015\ 0.011\ 0.011\ 0.011]^{\mathrm{T}}$, which characterizes the landing impact with vertical displacement and velocity. In addition, the initial states of the observers are identical to those of the corresponding LGSs. Irregular runway excitations to the front and main LGSs are generated by

$$\dot{z}_{fr} = \dot{z}_{mr} = \begin{cases} \frac{A}{2}(1 - \cos(\frac{2\pi V}{l}t)), & 0 \leqslant t \leqslant \frac{l}{V}, \\ 0, & \text{otherwise}, \end{cases}$$

where $A = 0.5$ m and $l = 2.5$ m are the height and length of the runway bump, $V = 20$ km/h is the taxiing velocity of the aircraft. The simulation results are plotted in Figures 3–7.

Figures 3 and 4 illustrate the actual, estimated, and transmitted states of the front and main LGSs, respectively. Furthermore, the actual and identified damping parameters of the front and main landing gears and wheels are presented in Figure 5. Figures 3–5 show that the designed adaptive observers can achieve the parameter identification of the landing gears and wheels, and the state estimation of the front and main LGSs is accurate even when the runway excitations are large, i.e., $A = 0.5$ m. The active suspension input and the internal ETM variable are depicted in Figure 6. Figure 7 shows the simulation results of the controlled outputs $\ddot{z}_a$ and $\ddot{\varphi}$ of the full aircraft LGS and the interevent time between two successive transmissions.

Moreover, a comparison between the proposed active control, e.g., active landing gear (ALG), and the traditional passive control, e.g., passive landing gear (PLG), is conducted to demonstrate the superiority of the proposed method in reducing vibrations. The left subfigure of Figure 7 and Table 2 show that the vertical and pitching acceleration of the aircraft fuselage can be substantially reduced using the active control method.

Furthermore, to verify the priority of the I-ETM strategy in saving network communication resources,

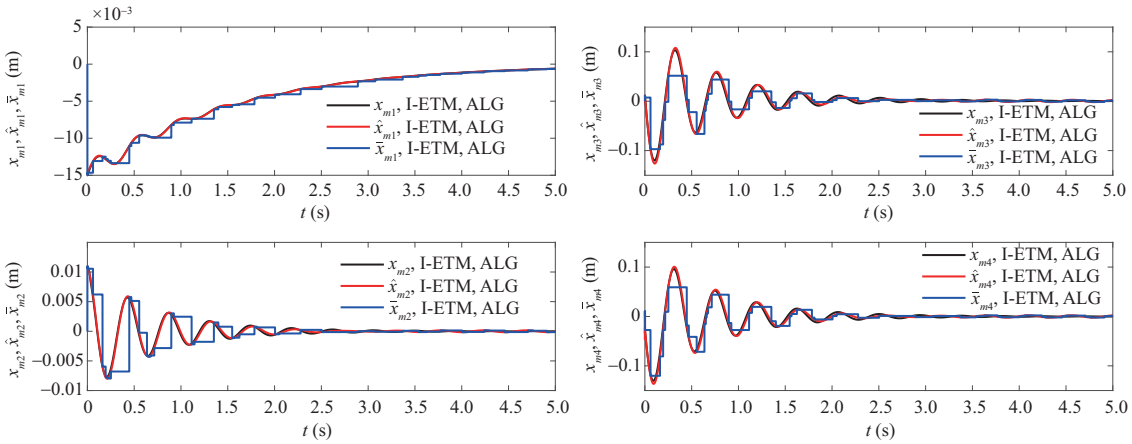

Figure 4 (Color online) Actual, estimated, and transmitted states of the main LGS.

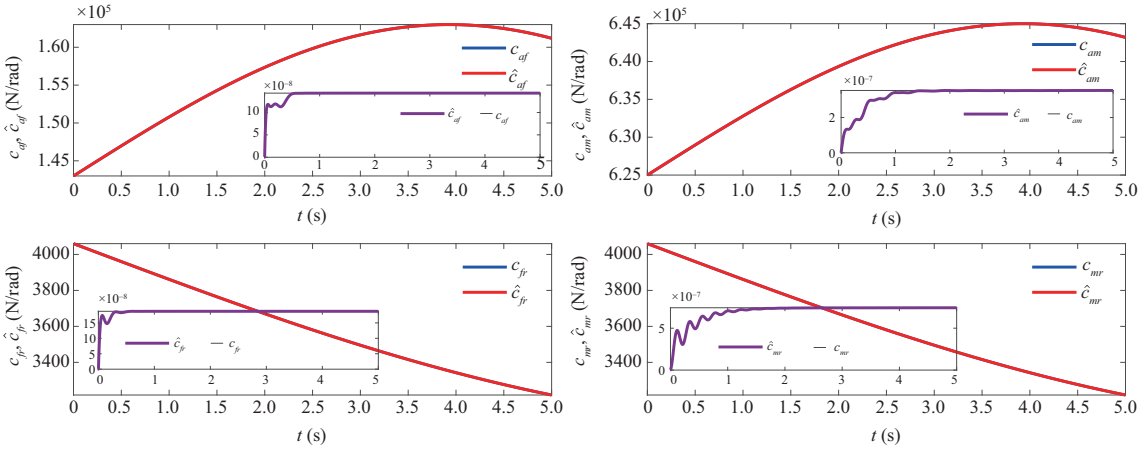

Figure 5 (Color online) Actual and identified damping parameters of the landing gears and wheels.

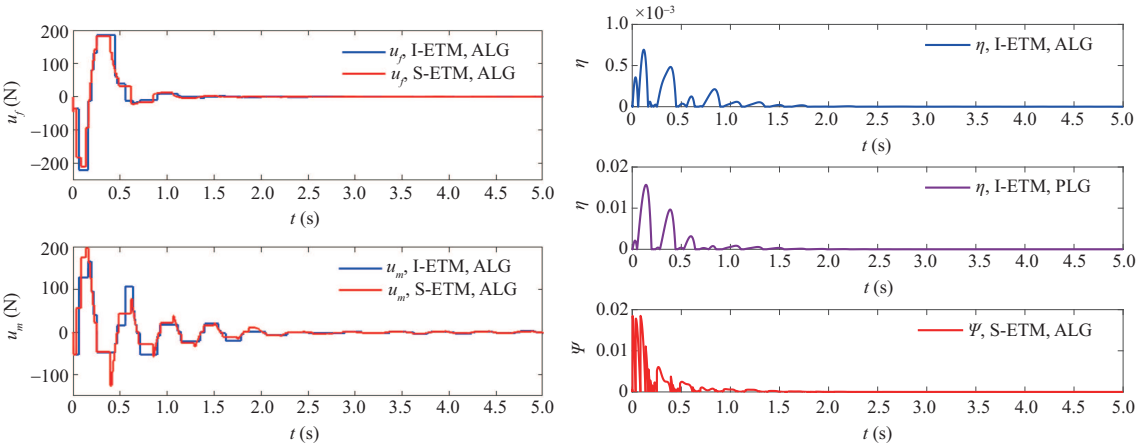

Figure 6 (Color online) Control input and ETM variables.

the performance of the LGS with active suspensions using the S-ETM is displayed, i.e.,

$$t_{k+1} = \inf\{(t - t_k \geqslant T \mid \Psi \leqslant 0) \text{ or } (t - t_k \geqslant \mathcal{T})\} \tag{28}$$

with $t_0 = 0$, $k \in \mathbb{Z}_{\geqslant 0}$, where $\Psi = \varepsilon \hat{x}^{\mathrm{T}} \hat{x} - \bar{\zeta}^2 W^2(e)$, and other parameters are identical to those in the I-ETM. The simulation results are shown in Figures 6 and 7. Furthermore, the minimum and average interevent time, the number of transmissions, and the occupancy rate of communication resources

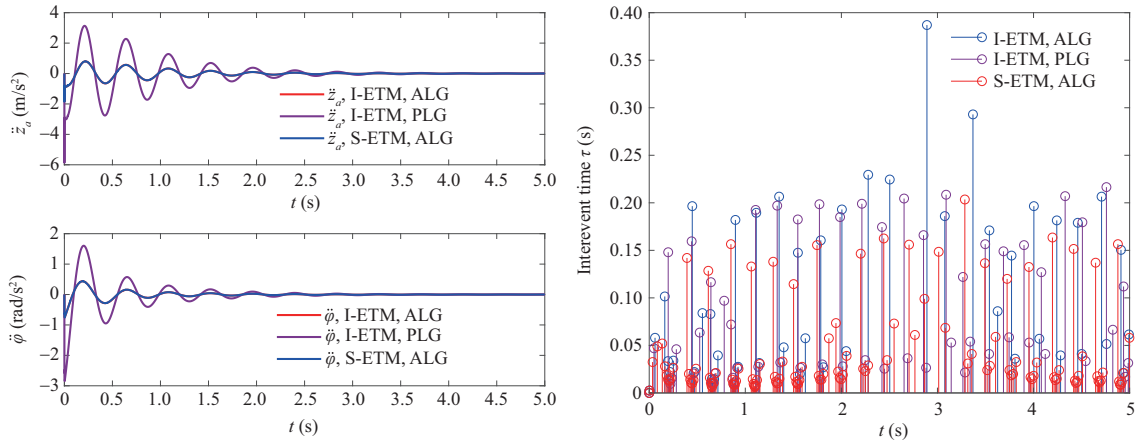

Figure 7 (Color online) Controlled output and interevent time.

Table 2 Comparisons of several methods

	T^{miet}	T^{avg}	$\lvert\ddot{z}_a\rvert_{\max}$	$\lvert\ddot{\varphi}\rvert_{\max}$	N	ORoCR (%)
I-ETM, ALG	0.0021	0.1064	1.8522	0.7547	47	0.47
I-ETM, PLG	0.0022	0.0847	5.8694	2.8461	59	0.59
S-ETM, ALG	0.0021	0.0424	1.8522	0.7547	118	1.18

(ORoCR) of the I-ETM and S-ETM for the full aircraft LGS with active suspensions, i.e., T^{miet}, T^{avg}, N, and ORoCR, are illustrated in Table 2. As depicted in Table 2, compared with the traditional periodic sampling mechanism, the integral and static ETMs substantially reduce the ORoCR, and the I-ETM saves more than half of the communication resources compared with the S-ETMs.

6 Conclusion

This article proposed a novel, robust adaptive observer-based integral event-triggered control method to achieve antivibration performance for a full aircraft ALG system under landing impact and runway excitations. First, the designed adaptive observers implemented the identification of the varying damping parameters and the system state estimation accurately and simultaneously. Second, the front and main subsystems were interconnected over a shared network through a novel integral event-triggered mechanism; thus, the overall networked control framework for the full aircraft LGS was constructed. Third, an integrated active controller with an adaptive law was synthesized based on the transmitted states of the front and main LGSs to guarantee the $\mathcal{L}_2$-stability of the augmented hybrid system. Furthermore, a codesign method was provided to obtain feasible solutions to the gain matrices of observers and controllers simultaneously. The simulation and comparison results demonstrated the effectiveness and superiority of the proposed control scheme in reducing the vertical and pitching vibrations of the landing impact and irregular runway excitations and saving communication resources. In the future, a valuable direction is to research the model-free reinforcement learning-based control method to achieve antivibration control for aircraft suspension systems with unknown parameters or dynamics in a model-free manner [35, 36].

Acknowledgements This work was supported by National Natural Science Foundation of China (Grant Nos. 62303492, 61973319), National Science Fund for Excellent Young Scholars of China (Grant No. 62222317), Postdoctoral Fellowship Program of CPSF (Grant Nos. BX20230430, 2023M733940), Science and Technology Major Project of Hunan Province (Grant No. 2021GK1030), Key R&D Plan of Hunan Province (Grant No. 2023GK2023), Science and Technology Innovation Program of Hunan Province (Grant No. 2022WZ1001), Natural Science Foundation of Hunan Province (Grant No. 2023JJ40765), and Natural Science Foundation of Changsha (Grant No. kq2208287).

References

1 Howe D. Aircraft Loading and Structural Layout. London: Professional Engineering Publishing, 2004
2 Ghiringhelli G L, Gualdi S. Evaluation of a landing gear semiactive control system for complete aircraft landing. Aerotecnica Missilie Spazio, 2004, 83: 21–31
3 Zhang H, Zheng X, Yan H, et al. Codesign of event-triggered and distributed H_∞ filtering for active semi-vehicle suspension systems. IEEE ASME Trans Mechatron, 2017, 22: 1047–1058
4 Zhang H, Hong Q, Yan H, et al. Event-based distributed H_∞ filtering networks of 2-DOF quarter-car suspension systems. IEEE Trans Ind Inf, 2016, 13: 312–321

5 Zapateiro M, Pozo F, Rossell J M, et al. Landing gear suspension control through adaptive backstepping techniques with H_∞ performance. IFAC Proc Volumes, 2011, 44: 4809–4814
6 Zhang H, Zheng X, Li H, et al. Active suspension system control with decentralized event-triggered scheme. IEEE Trans Ind Electron, 2020, 67: 10798–10808
7 Ge X, Ahmad I, Han Q L, et al. Dynamic event-triggered scheduling and control for vehicle active suspension over controller area network. Mech Syst Signal Processing, 2021, 152: 107481
8 Fei Z, Wang X, Liu M, et al. Reliable control for vehicle active suspension systems under event-triggered scheme with frequency range limitation. IEEE Trans Syst Man Cybern Syst, 2021, 51: 1630–1641
9 Yoon D S, Kim G W, Choi S B. Response time of magnetorheological dampers to current inputs in a semi-active suspension system: Modeling, control and sensitivity analysis. Mech Syst Signal Processing, 2021, 146: 106999
10 Wu Y, Ren G-P, Zhang H-T. Dual-mode predictive control of a rotor suspension system. Sci China Inf Sci, 2020, 63: 112204
11 Wen S, Chen M Z Q, Zeng Z, et al. Fuzzy control for uncertain vehicle active suspension systems via dynamic sliding-mode approach. IEEE Trans Syst Man Cybern Syst, 2016, 47: 24–32
12 Liu L, Li X, Liu Y J, et al. Neural network based adaptive event trigger control for a class of electromagnetic suspension systems. Control Eng Pract, 2021, 106: 104675
13 Gharapurkar A A, Jahromi A F, Bhat R B, et al. Semi-active control of aircraft landing gear system using H-infinity control approach. In: Proceedings of International Conference on Connected Vehicles and Expo (ICCVE), 2013. 679–686
14 Wang H, Xing J T, Price W G, et al. An investigation of an active landing gear system to reduce aircraft vibrations caused by landing impacts and runway excitations. J Sound Vib, 2008, 317: 50–66
15 Sivakumar S, Haran A P. Mathematical model and vibration analysis of aircraft with active landing gears. J Vib Control, 2015, 21: 229–245
16 Suresh P S, Sura N K, Shankar K. Investigation of nonlinear landing gear behavior and dynamic responses on high performance aircraft. J Aerospace Eng, 2019, 233: 5674–5688
17 Yazici H, Sever M. Observer based optimal vibration control of a full aircraft system having active landing gears and biodynamic pilot model. Shock Vib, 2016, 2016: 1–20
18 Chen Z Y, Han Q-L, Yan Y M, et al. How often should one update control and estimation: review of networked triggering techniques. Sci China Inf Sci, 2020, 63: 150201
19 Zhu S Y, Liu Y, Lou Y J, et al. Stabilization of logical control networks: an event-triggered control approach. Sci China Inf Sci, 2020, 63: 112203
20 Yu H, Hao F, Chen T. A uniform analysis on input-to-state stability of decentralized event-triggered control systems. IEEE Trans Automat Contr, 2019, 64: 3423–3430
21 Dolk V S, Borgers D P, Heemels W P M H. Output-based and decentralized dynamic event-triggered control with guaranteed $\mathcal{L}_p$-gain performance and zeno-freeness. IEEE Trans Automat Contr, 2017, 62: 34–49
22 Tabuada P. Event-triggered real-time scheduling of stabilizing control tasks. IEEE Trans Automat Contr, 2007, 52: 1680–1685
23 Heemels W P M H, Teel A R, van de Wouw N, et al. Networked control systems with communication constraints: tradeoffs between transmission intervals, delays and performance. IEEE Trans Automat Contr, 2010, 55: 1781–1796
24 Carnevale D, Teel A R, Nesic D. A Lyapunov proof of an improved maximum allowable transfer interval for networked control systems. IEEE Trans Automat Contr, 2007, 52: 892–897
25 Zhang Y F, Wu Z-G, Wu Z Z, et al. Resilient observer-based event-triggered control for cyber-physical systems under asynchronous denial-of-service attacks. Sci China Inf Sci, 2022, 65: 142203
26 Ma H, Li H Y, Lu R Q, et al. Adaptive event-triggered control for a class of nonlinear systems with periodic disturbances. Sci China Inf Sci, 2020, 63: 150212
27 Li H, Zhang Z, Yan H, et al. Adaptive event-triggered fuzzy control for uncertain active suspension systems. IEEE Trans Cybern, 2019, 49: 4388–4397
28 Wang X, Lemmon M D. Event design in event-triggered feedback control systems. In: Proceedings of the 47th IEEE Conference on Decision and Control, 2008. 2105–2110
29 Wang X, Lemmon M. On event design in event-triggered feedback systems. Automatica, 2011, 47: 2319–2322
30 Girard A. Dynamic triggering mechanisms for event-triggered control. IEEE Trans Automat Contr, 2015, 60: 1992–1997
31 Mousavi S H, Ghodrat M, Marquez H J. Integral-based event-triggered control scheme for a general class of non-linear systems. IET Control Theor & Appl, 2015, 9: 1982–1988
32 Mousavi S H, Ghodrat M, Marquez H J. A novel integral-based event triggering control for linear time-invariant systems. In: Proceedings of the 53rd IEEE Conference on Decision and Control, 2014. 1239–1243
33 Du C, Shi Y, Li F, et al. An improved co-design method of dynamical controller and asynchronous integral-type event-triggered mechanisms. IEEE Trans Syst Man Cybern Syst, 2023, 53: 2500–2509
34 Du C, Li F, Shi Y, et al. Integral event-triggered attack-resilient control of aircraft-on-ground synergistic turning system with uncertain tire cornering stiffness. IEEE CAA J Autom Sin, 2023, 10: 1276–1287
35 Mnih V, Kavukcuoglu K, Silver D, et al. Human-level control through deep reinforcement learning. Nature, 2015, 518: 529–533
36 Sutton R S, Barto A G. Reinforcement Learning: An Introduction. Cambridge: MIT Press, 2018